Asynchronous marine-terrestrial signals of the last deglacial warming in East Asia associated with low- and high-latitude climate changes

Deke Xu[a], Houyuan Lu[a,1], Naiqin Wu[a], Zhenxia Liu[b,c], Tiegang Li[d], Caiming Shen[e], and Luo Wang[a]

[a]Key Laboratory of Cenozoic Geology and Environment, Institute of Geology and Geophysics, Chinese Academy of Sciences, Beijing 100029, China; [b]First Institute of Oceanography and [c]Key Laboratory of Marine Science and Numerical Modeling, State Oceanic Administration, Qingdao 266061, China; [d]Institute of Oceanology, Chinese Academy of Sciences, Qingdao 266071, China; and [e]Key Laboratory of Plateau Lake Ecology and Global Change, Yunnan Normal University, Kunming, Yunnan 650092, China

A high-resolution multiproxy record, including pollen, foraminifera, and alkenone paleothermometry, obtained from a single core (DG9603) from the Okinawa Trough, East China Sea (ECS), provided unambiguous evidence for asynchronous climate change between the land and ocean over the past 40 ka. On land, the deglacial stage was characterized by rapid warming, as reflected by paleovegetation, and it began *ca.* 15 kaBP, consistent with the timing of the last deglacial warming in Greenland. However, sea surface temperature estimates from foraminifera and alkenone paleothermometry increased around 20–19 kaBP, as in the Western Pacific Warm Pool (WPWP). Sea surface temperatures in the Okinawa Trough were influenced mainly by heat transport from the tropical western Pacific Ocean by the Kuroshio Current, but the epicontinental vegetation of the ECS was influenced by atmospheric circulation linked to the northern high-latitude climate. Asynchronous terrestrial and marine signals of the last deglacial warming in East Asia were thus clearly related to ocean currents and atmospheric circulation. We argue that (*i*) early warming seawater of the WPWP, driven by low-latitude insolation and trade winds, moved northward via the Kuroshio Current and triggered marine warming along the ECS around 20–19 kaBP similar to that in the WPWP, and (*ii*) an almost complete shutdown of the Atlantic Meridional Overturning Circulation *ca.* 18–15 kaBP was associated with cold Heinrich stadial-1 and delayed terrestrial warming during the last deglacial warming until *ca.* 15 kaBP at northern high latitudes, and hence in East Asia. Terrestrial deglacial warming therefore lagged behind marine changes by *ca.* 3–4 ka.

asynchrony | East Asian monsoon | land-sea correlation | low- and high-latitude interplay | thermohaline circulation

Detailed knowledge of the phase relationships between climate changes in terrestrial and marine equatorial regions that link the Northern and Southern Hemispheres is critical to understanding the climate dynamics underlying orbital-scale and abrupt climate change (1–3). Previous research has focused on determining the relative timing of climate change during the last deglaciation between terrestrial and marine regions and/or between low- and high-latitude regions, with different conclusions:

i) Climate change in the continental Northern Hemisphere (4) was synchronous with that in the North Pacific Ocean (5), South China Sea (SCS) (6), Mediterranean Sea (7), and North Atlantic Ocean (8) during the last deglaciation. It was characterized by a rapid cooling at *ca.* 18–15 kaBP [Heinrich stadial-1 (HS1)] (9) and then an abrupt warming at *ca.* 15 kaBP (Bølling warm period) (10).

ii) Synchronous climate changes with a continuous warming from *ca.* 18 ± 1 to 10 kaBP occurred in Antarctica and high-latitude southern oceans, but this warming was interrupted by a minor pause or a slight cooling, called the Antarctic Cold Reversal (10–12). Temperature histories show that when a gradual cooling began in Antarctica, Greenland warmed abruptly. This

trading of heat between the hemispheres has been called the bipolar seesaw. It acts to redistribute heat depending on the state of the Atlantic Meridional Overturning Circulation (AMOC) (13).

iii) Climate change in tropical and middle-low latitudes of the Pacific Ocean, Indian Ocean, and South Atlantic Ocean was characterized by a continuous deglacial warming. This warming started at *ca.* 20–19 kaBP (3, 5, 9, 14), which is earlier than that in high latitudes of the Southern Hemisphere during the last deglacial period (9, 13, 14). It was not interrupted by any marked cooling event, such as the HS1 observed in high-latitude records of the Northern Hemisphere.

However, the vast majority of these results were acquired through comparisons of different proxy records from different materials with different resolution and dating uncertainties. Detailed knowledge concerning the leads and lags of climate changes between marine and terrestrial areas linking low and high latitudes is still controversial (15, 16).

Here, we present three sets of independent climate proxy data from a single core (DG9603) from the Okinawa Trough, East China Sea (ECS): one of terrestrial origin (pollen) and two of marine origin [foraminifera (17, 18) and alkenone paleothermometry ($U^{k'}_{37}$) (19, 20)]. The results provide robust evidence for oceanic and terrestrial environmental changes in East Asia during the past 40 ka. This study addresses the clear link between low-latitude oceanic and high-latitude terrestrial climate changes during the last deglacial warming.

Site Descriptions and Materials

Located in the eastern part of the ECS between the Pacific Ocean and the Eurasian continent, the Okinawa Trough is the only area that has continuously recorded environmental changes of both oceans and adjacent landmasses simultaneously. It thus provides direct and unambiguous evidence of the links between marine and terrestrial environments (21, 22).

The marine system in this region mainly consists of the Kuroshio Current (21, 22), which flows north on the western side of the North Pacific Ocean, analogous to the Gulf Stream in the North Atlantic Ocean. It transports about 3×10^7 m^3 of warm water per second from the tropical Pacific Ocean to the ECS

EARTH, ATMOSPHERIC, AND PLANETARY SCIENCES

region (21, 23). The epicontinental climate system is characterized by seasonal alterations of the East Asian summer and winter monsoons (24).

The ECS receives massive amounts of terrestrial sediments [about 2×10^9 tons/y (a)] transported by the Yangtze River and other rivers from the surrounding regions (25). During the Last Glacial Maximum (LGM), the ECS sea level was at least 125 m lower than at present; thus, most of the present shelf was exposed (22). The Okinawa Trough, close to the ECS shelf edge, has a water depth of more than 2,700 m in places and was continuously submerged during the glacial/interglacial cycles; thus, it continuously accumulated deposits of mixed terrestrial and marine sources.

Core DG9603 was taken from the mid-Okinawa Trough (28° 08.869'N, 127°16.238'E, water depth of 1,100 m) (Fig. 1). This 5.85-m core has continuous accumulation of semipelagic abyssal ooze with abundant microfossils, and the age model was established using accelerator mass spectrometry (AMS) ^{14}C dates (17, 18). Twelve samples for AMS ^{14}C dating were obtained from monospecific samples of the planktonic foraminifera *Globorotalia menardii*, *Globigerinoides sacculifer*, and *Neogloboquadrina dutertrei* (Table S1). The ^{14}C ages were converted to calendar ages using software CALIB 6.1 (26) and Marine09 datasets (27). The ages of samples from bottom to top were estimated by linear interpolation of these age control points. The top 4.5 m covers the past 42 ka, with an average resolution of *ca.* 208 a per sample.

Results

Vegetation Changes in Epicontinental Areas of the ECS. The relative abundance of subtropical evergreen arboreal taxa [*Quercus E* (evergreen) and *Castanopsis-Lithocarpus*], temperate arboreal taxa [*Quercus D* (deciduous)], and herbaceous species (Cyperaceae and *Artemisia*) revealed large (*ca.* 20–40%) and abrupt changes *ca.* 26.5 kaBP and *ca.* 15 kaBP (Fig. 2 and Figs. S1 and S2). Their absolute concentrations display similar changes (Fig. S3).

From *ca.* 26.5–15 kaBP, *Quercus D* rapidly increased, whereas *Quercus E* and *Castanopsis-Lithocarpus* significantly decreased. The maximum values of steppe and wetland taxa (*Artemisia* and Cyperaceae) and minimum values of the first principal component

Fig. 1. Overview maps of the Antarctic Ocean, Pacific Ocean, and Arctic Ocean, as well as the adjacent East Asia, showing locations of core DG9603 and selected paleoclimate sites in relation to oceanographic features. (*A*) Shown are the following: Greenland ice core North Greenland Ice Core Project (NGRIP) (31), Hulu cave (29), Dongge cave (30), marine core MD97-2138 (35), marine core MD03-2611 (36), marine core ODP 1233 (37), Antarctic ice core Taldice (12). (*B, Inset*) Map of the ECS and Yellow Sea shows a sketch of regional oceanic and atmospheric circulation. The location of core DG9603 is shown in the Okinawa Trough. All positions of paleoclimate sites related to this study are shown in red stars.

(F1) of principal components analysis (PCA) (*Methods*) indicate that the coldest climate occurred in this period during the past 40 ka. After *ca.* 15 kaBP, the sharp increase of tropical/subtropical evergreen arboreal taxa (i.e., *Quercus E*, *Castanopsis-Lithocarpus*), with a simultaneous decrease of *Quercus D* and herbaceous taxa, reflected a dramatic rise in temperature. Its timing coincided with an abrupt cold/warm and dry/wet transition observed in the Chinese cave stalagmites (29, 30) and in a Greenland ice core (31). A small increase in *Quercus D* and a slight decrease in *Quercus E* and *Castanopsis-Lithocarpus* during the interval from *ca.* 12.9–11.5 kaBP indicated a minor temperature reversal. The timing of this reversal corresponded with the cold Younger Dryas (YD) event. Notably, this temporal pattern of climate changes is similar to the last deglacial climate oscillation in the Greenland ice core (31) (Fig. 2).

Pollen in modern marine sediments of the ECS is derived from epicontinental vegetation along the adjacent eastern margin of China (32), from which location it is transported by rivers, winds, and long-shore currents and deposited in the ECS (33). Moreover, the exposed ECS shelf was also a major pollen source for the Okinawa Trough during the LGM and deglacial periods (32–34). Previous pollen records from the middle Okinawa Trough indicated that abrupt vegetation changes and land temperature increases were synchronous with the Bølling warm period warming observed in the Greenland ice core *ca.* 14.6 kaBP (34). Our evidence also corroborates this synchronous deglacial warming in the epicontinental climate of the ECS and northern high latitudes.

Asynchronous Marine and Terrestrial Signals During the Last Deglaciation. The high-resolution alkenone-based sea surface temperature (SST) (19, 20) record shows that a continual deglacial warming began around 20–19 kaBP, starting from the coldest estimated SST of 21 °C (i.e., about 5–6 °C lower than the modern SST; Fig. 3F). Similarly, the winter sea surface temperature (SSTw) reconstructed from fossil foraminiferal data of the same site using foraminiferal transfer functions (17, 18) yielded a comparable pattern for the last deglacial warming that started *ca.* 20–19 kaBP (Fig. 3G).

In both records, SSTw and $U^{k'}_{37}$ SST estimates had similar trends during the transition from the late glacial to the Holocene. However, the SSTw curve showed a relatively larger amplitude of SSTw variation than $U^{k'}_{37}$ SST, because the foraminiferal transfer function has a higher sensitivity than alkenone methodologies (5). Notably, the pattern of this transition was similar to that of the last deglacial warming recorded in marine core from the Western Pacific Warm Pool (WPWP) (35) (Fig. 3H), suggesting a direct link in SST changes between the Okinawa Trough and the tropical Pacific Ocean. In addition, temperature records from the southern Pacific Ocean (36, 37) (Fig. 3 *I* and *J*) and the Antarctic region (12) (Fig. 3K) showed that a continual deglacial warming began at *ca.* 19–18 kaBP, slightly lagging behind that of the WPWP on the Greenland Ice Core Chronology 2005 (GICC05) time scale (11, 12).

In contrast to marine signals of climate change with an early onset of the last deglacial warming *ca.* 20–19 kaBP, the terrestrial signals of the last deglacial climate changes, as evidenced by the paleovegetation changes reconstructed from the pollen record of core DG9603, clearly indicated that abrupt warming began *ca.* 15 kaBP. This late onset of warming in the terrestrial record is consistent with the last deglacial warming pattern reflected in the $\delta^{18}O$ records from the Hulu Cave and Dongge Cave stalagmites in eastern China (29, 30), as well as in the Greenland ice core (31).

Our study therefore revealed the occurrence of asynchronous marine and terrestrial signals of climate change in East Asia. Our findings are based on three independent lines of evidence (terrestrial and marine records) obtained from the same core; thus,
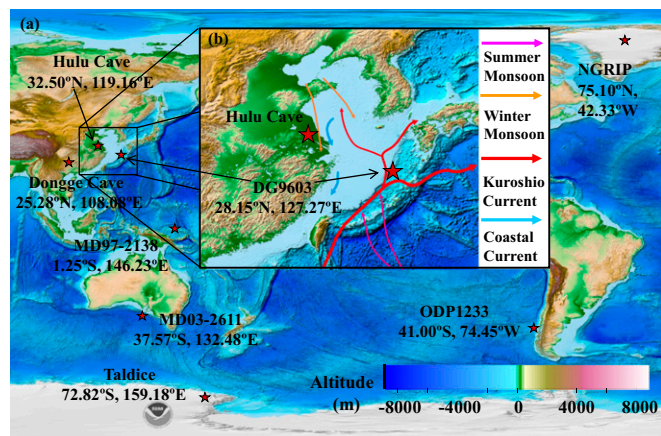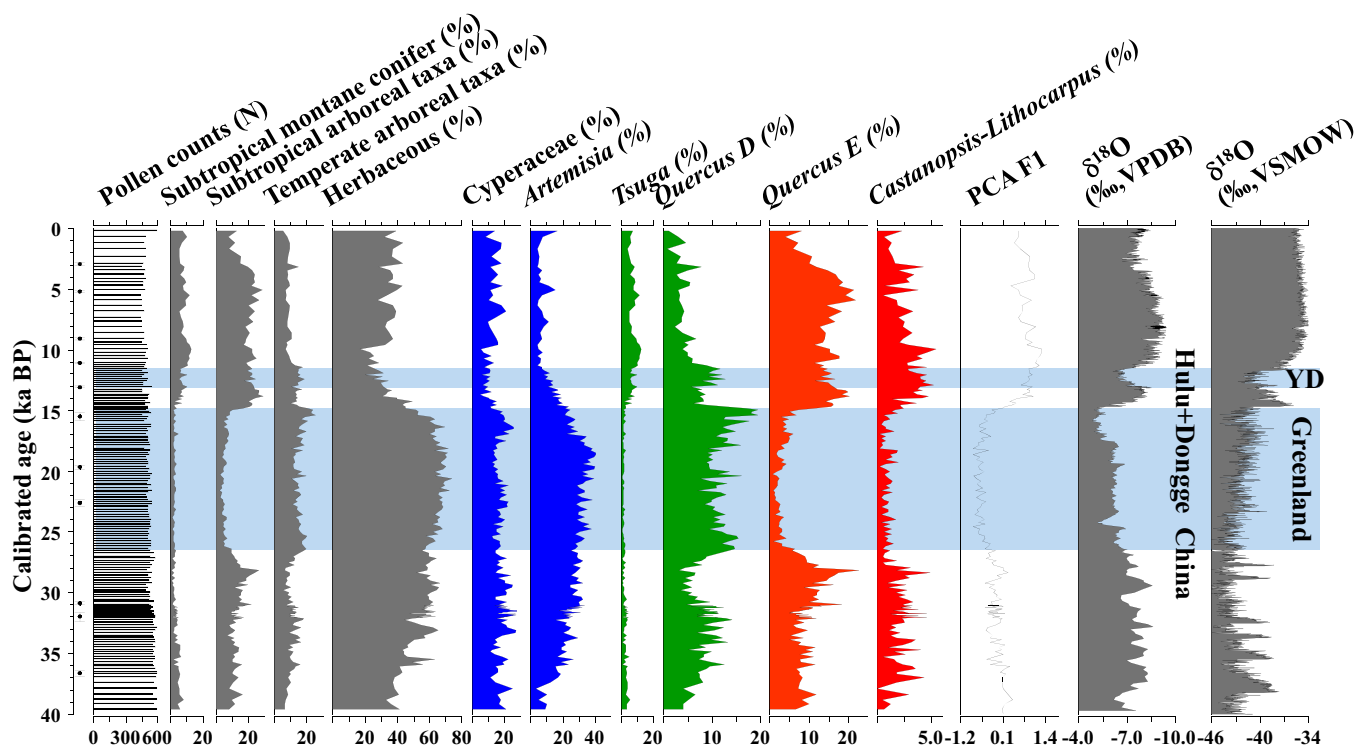
Fig. 2. Diagram of selected pollen types from core DG9603, together with $\delta^{18}O$ records from the Greenland ice core (31) [on a GICC05 time scale (28)] and cave stalagmites (29, 30) of East Asia. Calibrated ages are shown by black dots with 1σ uncertainty on the left axis of the pollen diagram. Two blue-shaded bars show the YD and the cold period from *ca.* 26.5–15 kaBP, respectively. VPDB, Vienna Peedee Belemnite; VSMOW, Vienna Standard Mean Ocean Water.

they avoid the pitfall of age uncertainties arising from correlations of proxy records obtained from different cores with different radiocarbon dating controls. The timing of oceanographic changes in the ECS significantly led the corresponding variations in its epicontinental vegetation and climate by about 3–4 ka on glacial/interglacial time scales (Fig. 3).

Discussion and Conclusions

Vegetation Changes and the East Asian Monsoon. The East Asian monsoon is a dynamic, interactive climate system driven by two seasonally reversing mechanisms. In summer, the differential heating produces an atmospheric pressure gradient between an ocean and continent that forces a steady flow of warm and moist maritime air onto the continent (i.e., the East Asian summer monsoon). In winter, the atmospheric pressure gradient is reversed, resulting in the flow of cold, dry air out from north-central Asia (i.e., the winter monsoon). Vegetation changes on the East Asian continent are mainly controlled by these two monsoon seasons (33, 34). Because the plant community response to climate changes is very rapid, probably within a few decades (38, 39), a high-resolution pollen record derived from core DG9603 revealed not only vegetation but Asian monsoon changes in epicontinental areas of the ECS.

From *ca.* 40–26.5 kaBP, these areas were covered by warm temperate forest-steppe and wetlands, indicating a relatively strong summer monsoon. During the period of ~26.5–15 kaBP, wetland and temperate steppe (or a mosaic of forest and grassland) developed, reflecting a stronger winter monsoon. In this period, a gradual reduction of *Artemisia* occurred from *ca.* 18–15 kaBP. As shown in Fig. 2 and Fig. S2, *Artemisia* pollen was mainly replaced during this period by Cyperaceae and *Quercus D*, which have ecological and climatic implications relative to *Artemisia* in the pollen record, suggesting no major change in epicontinental vegetation types and climate before and after 18 kaBP. This gradual

reduction of *Artemisia* might be ascribed to the shrinking of the grass-covered ECS continental shelf due to the rise of the deglacial sea level (33, 34) rather than to climate change. The exposed continental shelf was composed mainly of saline sandy soil favorable to the growth of *Artemisia* (40); thus, the gradual decrease of *Artemisia* in deglacial sediments likely reflected the process of marine transgression on the previously exposed shelf (34, 40). It is evident that the sudden change of vegetation and climate occurred around 15 kaBP, as indicated by clear changes in the PCA F1 scores and the abrupt shift in zonal vegetation types (Fig. 2). Northern subtropical forest quickly developed from *ca.* 15 kaBP to the early-middle Holocene, corresponding to the rapid strengthening of the Asian summer monsoon, as reflected in the $\delta^{18}O$ records of stalagmites in eastern China (29, 30). Furthermore, this rapid transition was nearly synchronous with the last deglacial warming in the Greenland ice core. Previous studies indicated that fluctuations in the East Asian monsoon were almost synchronous with the fast and drastic temperature changes in the Northern Hemisphere (29). Therefore, our results further demonstrate this relationship between the East Asian monsoon dynamics and northern high-latitude climate change (29, 41).

Tropical Pacific Ocean Plays a Key Role in Regulating SST Variations in the ECS. Based on a compilation of currently available records of past SST, the regional-scale deglacial SST development in the Pacific Ocean was tentatively classified into four end-member types (5). Among them, the subtropical and tropical Pacific Ocean type (including WPWP) was characterized by a continuous deglacial warming without any marked interruption during the time intervals of the YD and HS1. All tropical and subtropical Pacific Ocean SST records show an onset of the last deglacial warming at *ca.* 20–19 kaBP (5, 9). In the ECS, the other existing $U^{k'}_{37}$ SST record from the northern region of the
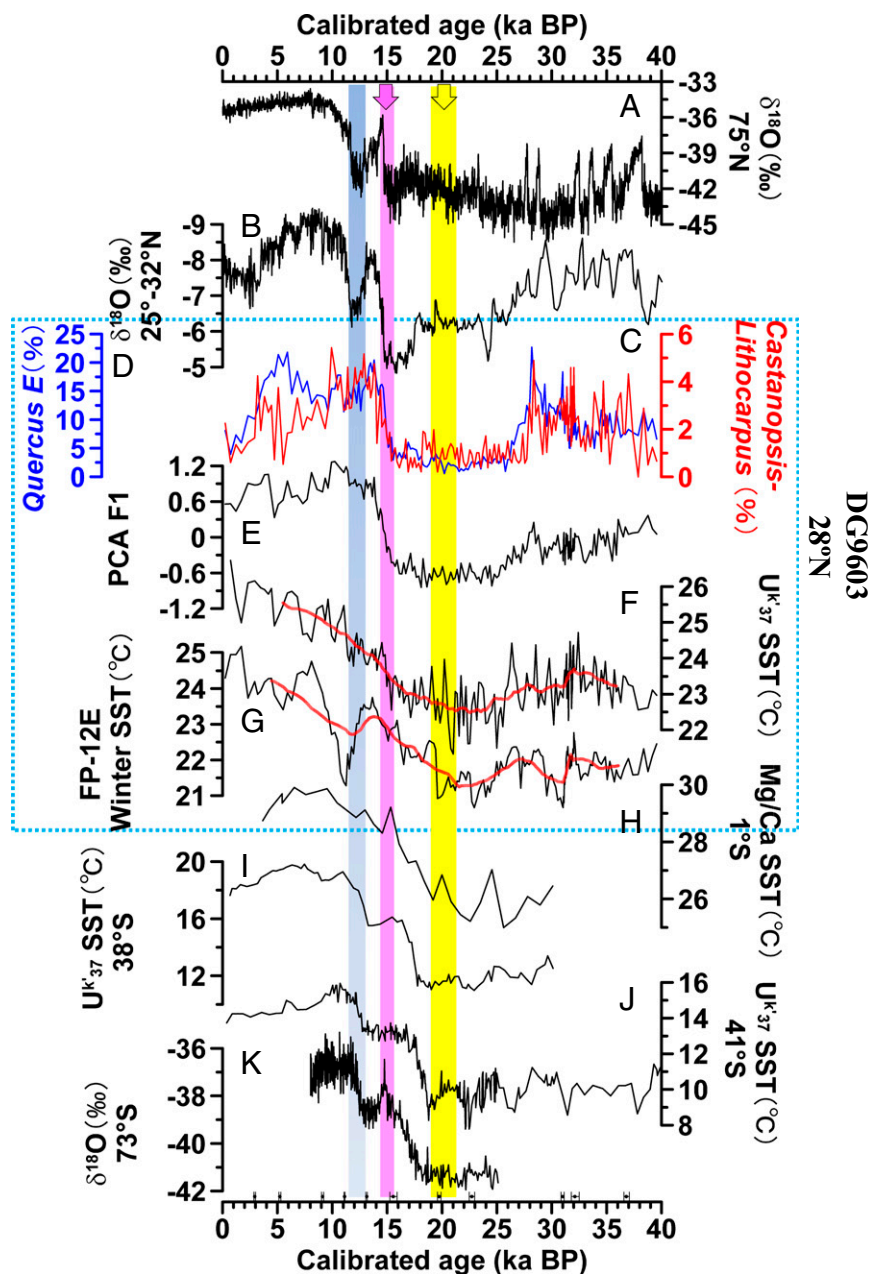
Fig. 3. Comparison of deglacial climate proxy records from core DG9603 with other proxy records for temperature and circulation in the Antarctic Ocean, Pacific Ocean, Greenland, and East Asia. $\delta^{18}O$ record from the NGRIP (31) [on a GICC05 time scale (28)] (*A*), $\delta^{18}O$ records from Hulu and Dongge caves (29, 30) (*B*), multiproxy records of core DG9603 in the dashed blue box [*Castanopsis-Lithocarpus* (*C*), *Quercus E* (*D*), PCA F1 (*E*), $U^{k'}_{37}$ SST (19, 20) (*F*), and FP-12E SSTw (18) (*G*)], Mg/Ca SST in MD97-2138 core (35) (*H*), $U^{k'}_{37}$ SST in MD03-2611 core (36) (*I*), $U^{k'}_{37}$ SST in ODP1233 core (37) (*J*), and $\delta^{18}O$ record from Taldice (on a GICC05 time scale) (12) (*K*). Black dots at the bottom indicate dating control points with 1σ uncertainty for the DG9603 core. The yellow-shaded bar (arrow) and pink-shaded bar (arrow) show the timing of the last deglacial warming in SST records from the WPWP (*H*) and ECS (*F* and *G*), and in terrestrial climate records from East Asia (*B*–*D*) and Greenland (*A*), respectively; the blue-shaded bar shows the YD cold period. Red lines in *F* and *G* are 25-point running averages.

Okinawa Trough also displayed a continuous deglacial warming pattern beginning at *ca.* 19 kaBP (42).

Understanding the cause of the continuous deglacial SST warming of the Kuroshio region that started *ca.* 20–19 kaBP offers important insights into the mechanisms for a linkage between the ECS and the tropical Pacific Ocean. The $\delta^{13}C$ record of planktonic foraminifera from the Kuroshio region showed a broad minimum during the last deglaciation in the Okinawa Trough (43). This event was consistent with the last deglacial $\delta^{13}C$ minimum in records from the western equatorial Pacific Ocean, which suggests that the source water may have come from the tropical Pacific Ocean during the last deglaciation (43). Because the last deglacial $\delta^{13}C$ minimum in records from the western equatorial Pacific Ocean was an important regional paleoceanographic event (43), the consistency in the timing of this event between two regions implies that signals from the tropical zone of the ocean can be rapidly delivered to the northern middle latitudes along the path of the Kuroshio region. It also suggests that warming

water evolution in the tropical Pacific Ocean played a key role in regulating SST variations of the ECS (43, 44).

A comparison of our SST records with those in the SCS showed that SST in the Okinawa Trough was influenced more significantly by SST changes in the tropical Pacific Ocean during the last deglaciation. The SCS, consisting of semienclosed marginal basins, was unlikely to be affected by Pacific Ocean open circulation, especially in the glacial period with a low sea level (6). It was more vulnerable to being influenced by the East Asian monsoon associated with high-latitude atmospheric circulation (45, 46).

Asynchronous Marine and Terrestrial Signals Associated with Low- and High-Latitude Climate Changes. Low-latitude tropical regions (*ca.* 23°N–23°S) receive about half of the solar energy on the Earth's surface (47, 48); the tropical ocean is therefore considered as the "heat engine" driving the global climate system on seasonal to geological time scales (49). However, what mechanisms caused the last deglacial warming that started at *ca.* 20–19

kaBP in the WPWP and its spreading from low-latitude oceans to high-latitude northern and southern oceans?

Shiau and Chen (46) found that the SST warming in the tropical regions at *ca.* 20–19 kaBP was synchronous with the increase of June local solar radiation at *ca.* 20 kaBP. This correspondence with the precessional cycle suggests that insolation could be the main factor responsible for early SST warming (46). De Deckker et al. (1) recently proposed another mechanism: An early phase of the last deglacial warming in the WPWP probably resulted from maximum austral summer insolation peaking at 21 kaBP (1), which stored a large amount of heat in the WPWP.

However, the heat storage in the WPWP may also be affected by other factors, especially the trade winds (47, 49, 50). Under the trade wind stress, the thermocline is deep in the West and shallow in the East; thus, a huge amount of heat is stored in the tropical western Pacific Ocean by the westward warm equatorial current, creating the WPWP. Geological records (51) and model simulations (52) revealed that SST increase in the WPWP was consistent with the strengthened intensity of trade winds, as the summer (June, July, August) solar radiation increased from 20 kaBP under the precessional cycle (47, 50–52). Therefore, the last deglacial warming beginning as early as *ca.* 20 kaBP in the WPWP was mainly driven by the tropical insolation and trade wind intensity (46, 52, 53).

With an excess of heat stored in the WPWP *ca.* 20 kaBP, the heat would have been transferred from low to high latitudes by the assistance of surface ocean currents. In the north of the WPWP, the warming water was moved northward by the Kuroshio Current to enter the ECS. This process led to the ECS warming *ca.* 20–19 kaBP, at the same time as in the WPWP. On the southern margin of the WPWP, the southward shift of the subtropical front and the rise in sea level allowed the stored heat in the WPWP to flow into the central Indian Ocean and then to escape into the Atlantic Ocean via the Agulhas Current, as De Deckker et al. (1) have proposed. The huge influx of warm saltwater into the Atlantic Ocean may have ultimately helped to restore a vigorous AMOC, which could further affect climate change in high latitudes of the Northern Hemisphere (1, 54).

Previous studies have shown that the temperature started to increase *ca.* 20–19 kaBP with an increase in summer radiation at high latitudes of the Northern Hemisphere (10). The vast ice sheets subsequently began to melt *ca.* 19 kaBP. The huge quantities of fresh water pouring into the North Atlantic Ocean would have diluted the salty water, making it less dense, which resulted in variability in strength of the AMOC. Furthermore, an almost complete shutdown of the AMOC *ca.* 18–15 kaBP would have resulted in much less heat being carried northward by the surface currents, and thus cooling of the Northern Hemisphere (HS1) (10, 13, 44, 55, 56). The HS1 has been widely documented in a variety of proxy records in the Northern Hemisphere (10, 29, 30, 56), and it delayed warming in the Northern Hemisphere until *ca.* 15 kaBP. Therefore, the last terrestrial deglacial warming in East Asia lagged *ca.* 3–4 ka behind that of SST in the ECS and tropical western Pacific Ocean.

Overall, our results provide robust evidence for asynchronous marine and terrestrial signals of climate changes during the last deglaciation in East Asia. The timing of oceanographic changes significantly led to the corresponding variations in epicontinental vegetation and climate by about 3–4 ka. We suggest that this asynchrony was related to the early warming of seawater in the WPWP, which moved northward into the ECS via the Kuroshio Current, where it encountered Northern Hemisphere terrestrial cooling associated with the cold HS1.

The East Asian coastal margin serves as a boundary region between two regional climate systems, one governed by the high-latitude Northern Hemisphere climate and the other governed by the low-latitude ocean climate. These two oceanic and terrestrial climate components modulate the East Asian climate.

Although this study shows remarkable asynchronous climate changes between East Asia land and the adjacent oceans, this finding is probably limited to the region influenced by the Kuroshio Current, because the ocean and surrounding terrestrial regions located north of the Kuroshio Current were affected by the high-latitude Northern Hemisphere climate changes during the last deglaciation (5, 57). It is clear that more investigations are required to derive more precise climate reconstructions in both the marine and terrestrial realms because of complicated interactions of ocean currents and the atmospheric system.

Moreover, the physical mechanisms of asynchronous changes in the climate systems in East Asia are not yet included in paleoclimate or present-day coupled oceanic-atmospheric models. If an accurate representation of the leads and lags between marine and terrestrial signals of climate changes is obtained, it could substantially improve the predictive skill of climate models. This is crucial to a better understanding of East Asia monsoon dynamics associated with low- and high-latitude climate changes and interactions.

Methods

The analysis of pollen, foraminifera (17), and $U^{k'}_{37}$ (19, 20) was conducted on the same number of samples ($n = 204$), which were collected at the same intervals (2–3 cm) from the top 4.5 m of core DG9603 (Tables S2 and S3).

Previously, relatively coarse and short pollen records (20–30 kaBP) from this core have been reported (16, 32). For this study, this core was comprehensively resampled to improve the resolution of the crucial last deglaciation section of the profile and extend temporal coverage over the past 42 kaBP. Pollen analysis was undertaken on all samples using a standard procedure: 3.0-g samples were prepared to extract pollen and spores using standard potassium hydroxide and hydrofluoric acid digestion; a total of at least 450 (average of 528) pollen grains and spores were counted for each sample. Using C2 software (58), PCA was applied to the terrestrial pollen percentage data to extract the main gradient changes in vegetation. Pollen percentages were square root-transformed before numerical analyses to stabilize their variances. All pollen taxa with a relative abundance >2% in at least two samples were used in data analyses. The first and second principal components (PCA F1 and PCA F2) have eigenvalues of 0.31 and 0.11, respectively.

Subtropical evergreen taxa, especially *Quercus E* and *Castanopsis-Lithocarpus*, have the highest positive loadings on axis 1, whereas the temperate deciduous taxon *Quercus D*, as well as *Artemisia*, Cyperaceae, Gramineae, Chenopodiaceae, and Compositae, have negative loadings, indicating a gradient from warm (positive loadings) to cold (negative loadings) climate conditions (Fig. S1).

Foraminifera Extraction. Each sample was soaked in water for 2 h and then washed through a 63-μm sieve. Foraminifera were identified, sorted, and counted from size fractions larger than 150 μm. Almost all foraminifera smaller than 150 μm are juveniles and cannot be readily identified. To reduce statistical error, all specimens (a minimum of 367 shells) in the samples were identified and counted. Transfer function FP-12E was applied to fossil foraminifera data to estimate the SSTw quantitatively.

Alkenone-Derived SSTs. The procedures and equipment used for the lipid determination are described elsewhere (19, 20). Briefly, sediment samples were first freeze-dried and manually ground for homogeneity; lipids were subsequently extracted with 3:1 CH_2Cl_2/CH_3OH; and the extract was rotary-evaporated and concentrated, and then separated by TLC. The samples treated by extraction were emersed in CH_2Cl_2 again for the next measurement. The ketone components with rf ranging from 0.45 to 0.8 were selected from lipid compounds for GC and GC/MS/MS.

Lipid extracts were analyzed using an HP5880A (Agilent) gas chromatograph equipped with an elastic silica capillary column (25 m × 0.2 mm) and SE-54 (Chrome) fixing solution. Samples were injected onto the column at 100 °C and programmed to run at 4 to 290 °C/min with N_2 as the carrier gas. GC/MS/MS analysis was conducted using a MAT TSQ70B (Finnigan) mass spectrometer equipped with an elastic silica capillary column [30 m × 0.25 mm, smeared with DB1 (J&W)]. The GC/MS/MS was programmed at 120–130 °C with a rising rate of 3 °C/min, and it was run with electron energy (70 eV, 200-μA emission current). Using the peak area of each lipid molecule on the chromatogram as its relative concentration, the alkenone unsaturation ratio $U^{k'}_{37}$ was calculated. The SST was reconstructed using the formula $U^{k'}_{37} = 0.031T + 0.092$, as corrected by Pelejero and Grimalt (59).

1. De Deckker P, Moros M, Perner K, Jansen E (2012) Influence of the tropics and southern westerlies on glacial interhemispheric asymmetry. *Nat Geosci* 5(4): 266–269.
2. Jennerjahn TC, et al. (2004) Asynchronous terrestrial and marine signals of climate change during Heinrich events. *Science* 306(5705):2236–2239.
3. Barker S, et al. (2009) Interhemispheric Atlantic seesaw response during the last deglaciation. *Nature* 457(7233):1097–1102.
4. Clark PU, et al. (2009) The Last Glacial Maximum. *Science* 325(5941):710–714.
5. Kiefer T, Kienast M (2005) Patterns of deglacial warming in the Pacific Ocean: A review with emphasis on the time interval of Heinrich event 1. *Quat Sci Rev* 24(7-9): 1063–1081.
6. Kienast M, Steinke S, Stattegger K, Calvert SE (2001) Synchronous tropical South China Sea SST change and Greenland warming during deglaciation. *Science* 291(5511):2132–2134.
7. Castañeda IS, et al. (2010) Millennial-scale sea surface temperature changes in the eastern Mediterranean (Nile River Delta region) over the last 27,000 years. *Paleoceanography* 25(1):PA1208.
8. Benson L, Burdett J, Lund S, Kashgarian M, Mensing S (1997) Nearly synchronous climate change in the Northern Hemisphere during the last glacial termination. *Nature* 388(6639):263–265.
9. Clark PU, et al. (2012) Global climate evolution during the last deglaciation. *Proc Natl Acad Sci USA* 109(19):E1134–E1142.
10. Denton GH, et al. (2010) The last glacial termination. *Science* 328(5986):1652–1656.
11. Pedro JB, et al. (2011) The last deglaciation: Timing the bipolar seesaw. *Clim Past* 7(2): 671–683.
12. Stenni B, et al. (2011) Expression of the bipolar see-saw in Antarctic climate records during the last deglaciation. *Nat Geosci* 4(1):46–49.
13. Stocker TF, Johnsen SJ (2003) A minimum thermodynamic model for the bipolar seesaw. *Paleoceanography* 18(4):1087.
14. Shakun JD, et al. (2012) Global warming preceded by increasing carbon dioxide concentrations during the last deglaciation. *Nature* 484(7392):49–54.
15. Lea DW, Pak DK, Spero HJ (2000) Climate impact of late quaternary equatorial pacific sea surface temperature variations. *Science* 289(5485):1719–1724.
16. Lu HY, et al. (2002) Asynchrony of the marine and epicontinental climate records in the East Asia during the last 20 ka. *Mar Geol Quat Geol* 22(1):17–23.
17. Li TG, et al. (2001) Heinrich event imprints in the Okinawa Trough: Evidence from oxygen isotope and planktonic foraminifera. *Palaeogeogr Palaeoclimatol Palaeoecol* 176(1-4):133–146.
18. Liu ZX, et al. (2001) The paleoclimatic events and cause in the Okinawa Trough during 50 kaBP. *Chin Sci Bull* 46(2):153–157.
19. Meng XW, Du DW, Liu YG, Liu ZX (2002) Molecular biomarker record of paleoceanographic environment in the East China Sea during the last 35,000 years. *Science in China Series D Earth Science* 45(2):184–192.
20. Xiong YQ, Liu ZX (2004) Variations in sediment provenance and its implications of Core DGKS9603 since the late Quaternary. *Acta Oceanol Sin* 26(2):61–71.
21. Wang PX (1985) *Marine Micropaleontology of China* (China Ocean Press, Beijing).
22. Saito Y, et al. (1998) Transgressive and highstand systems tracts and post-glacial transgression, the East China Sea. *Sediment Geol* 122(1-4):217–232.
23. Zhao B, Fang G (1991) The estimation of the flow of main waterways in the East China Sea. *Acta Oceanol Sin* 13(2):169–177.
24. Yancheva G, et al. (2007) Influence of the intertropical convergence zone on the East Asian monsoon. *Nature* 445(7123):74–77.
25. Hu D, Saito Y, Kempe S (1998) Sediment and nutrient transport to the coastal zone. *Asian Change in the Context of Global Climate Change: Impact of Natural and Anthropogenic Changes in Asia on Global Biogeochemical Cycles*, eds Galloway JN, Melillo JM (Cambridge Univ Press, Cambridge, UK), pp 245–270.
26. Stuiver M, et al. (1998) INTCAL98 radiocarbon age calibration, 24,000-0 cal BP. *Radiocarbon* 40(3):1041–1083.
27. Reimer PJ, et al. (2009) IntCal09 and Marine09 radiocarbon age calibration curves, 0-50,000 years cal BP. *Radiocarbon* 51(4):1111–1150.
28. Andersen KK, et al. (2006) The Greenland Ice Core Chronology 2005, 15–42 ka. Part 1: Constructing the time scale. *Quat Sci Rev* 25(23-24):3246–3257.
29. Wang YJ, et al. (2001) A high-resolution absolute-dated late Pleistocene Monsoon record from Hulu Cave, China. *Science* 294(5550):2345–2348.
30. Dykoski C, et al. (2005) A high-resolution, absolute-dated Holocene and deglacial Asian monsoon record from Dongge Cave, China. *Earth Planet Sci Lett* 233(1-2): 71–86.
31. Andersen KK, et al.; North Greenland Ice Core Project members (2004) High-resolution record of Northern Hemisphere climate extending into the last interglacial period. *Nature* 431(7005):147–151.
32. Xu D, Lu H, Wu N, Liu Z (2010) 30,000-Year vegetation and climate change around the East China Sea shelf inferred from a high-resolution pollen record. *Quat Int* 227(1):53–60.
33. Wang KF, Sun YH, Zhang YL, Jiang H, Zhang YC (1987) *The Spore-Pollen and Algal Assemblage in the East China Sea Sediments* (China Ocean Press, Beijing).
34. Zheng Z, et al. (2011) Pollen record of the past 60 ka BP in the Middle Okinawa Trough: Terrestrial provenance and reconstruction of the paleoenvironment. *Palaeogeogr Palaeoclimatol Palaeoecol* 307(1-4):285–300.
35. de Garidel-Thoron T, et al. (2007) A multiproxy assessment of the western equatorial Pacific hydrography during the last 30 kyr. *Paleoceanography* 22(3): PA3204.
36. Calvo E, Pelejero C, De Deckker P, Logan GA (2007) Antarctic deglacial pattern in a 30 kyr record of sea surface temperature offshore South Australia. *Geophys Res Lett* 34(13):L13707.
37. Kaiser J, Lamy F, Hebbeln D (2005) A 70-kyr sea surface temperature record off southern Chile (Ocean Drilling Program Site 1233). *Paleoceanography* 20(4):PA4009.
38. Ritchie JC (1986) Climate change and vegetation response. *Plant Ecol* 67(2): 65–74.
39. Stebich M, Mingram J, Han J, Liu J (2009) Late Pleistocene spread of (cool-)temperate forests in Northeast China and climate changes synchronous with the North Atlantic region. *Global Planet Change* 65(1-2):56–70.
40. Sun XJ, Li X, Luo YL, Chen XD (2000) The vegetation and climate at the last glaciation on the emerged continental shelf of the South China Sea. *Palaeogeogr Palaeoclimatol Palaeoecol* 160(3-4):301–316.
41. Taylor KC, et al. (1997) The Holocene-Younger Dryas transition recorded at Summit, Greenland. *Science* 278(5339):825–827.
42. Ijiri A, et al. (2005) Paleoenvironmental changes in the northern area of the East China Sea during the past 42,000 years. *Palaeogeogr Palaeoclimatol Palaeoecol* 219(3-4):239–261.
43. Li TG, et al. (2002) A broad deglacial delta C-13 minimum event in planktonic foraminiferal records in the Okinawa Trough. *Chin Sci Bull* 47(7):599–603.
44. Pierrehumbert RT (2000) Climate change and the tropical Pacific: The sleeping dragon wakes. *Proc Natl Acad Sci USA* 97(4):1355–1358.
45. Oppo DW, Sun Y (2005) Amplitude and timing of sea-surface temperature change in the northern South China Sea: Dynamic link to the East Asian monsoon. *Geology* 33(10):785–788.
46. Shiau LJ, Chen MT (2011) The climate dynamics of the Western Pacific warm pool on the millennial to orbital time scales. *J Earth Sci Environ* 2(5):569–604.
47. Li KR (1993) *China Sea and Northwest Pacific Ocean climate* (China Ocean Press, Beijing).
48. Berger A (2009) Monsoon and general circulation system. *Chin Sci Bull* 54(7):1111–1112.
49. Wang PX (2009) Global monsoon in a geological perspective. *Chin Sci Bull* 54(7): 1113–1136.
50. Wang PX (2006) Orbital forcing of the low latitude processes. *Quat Sci* 26(5): 694–701.
51. Koutavas A, Lynch-Stieglitz J, Marchitto TM, Jr., Sachs JP (2002) El Niño-like pattern in ice age tropical Pacific sea surface temperature. *Science* 297(5579):226–230.
52. Clement AC, Seager R, Cane MA (1999) Orbital controls on the El Nino/Southern Oscillation and the tropical climate. *Paleoceanography* 14(4):441–456.
53. McIntyre A, Molfino B (1996) Forcing of Atlantic Equatorial and Subpolar Millennial Cycles by Precession. *Science* 274(5294):1867–1870.
54. Beal LM, De Ruijter WPM, Biastoch A, Zahn R; SCOR/WCRP/IAPSO Working Group 136 (2011) On the role of the Agulhas system in ocean circulation and climate. *Nature* 472(7344):429–436.
55. Broecker WS, et al. (1989) Routing of meltwater from the Laurentide Ice Sheet during the Younger Dryas cold episode. *Nature* 341(6240):318–321.
56. Broecker WS, et al. (2010) Putting the Younger Dryas cold event into context. *Quat Sci Rev* 29(9-10):1078–1081.
57. Kawahata H, Ohshima H, Kuroyanagi A (2011) Terrestrial– ocean environmental change in the northwestern Pacific from the glacial times to Holocene. *J Asian Earth Sci* 40(6):1189–1202.
58. Juggins S (2003) *C2 User Guide: Software for Ecological and Palaeoecological Data Analysis and Visualisation* (Univ of Newcastle, Newcastle upon Tyne, UK).
59. Pelejero C, Grimalt JO (1997) The correlation between the 37k index and sea surface temperatures in the warm boundary: The South China Sea. *Geochim Cosmochim Acta* 61(22):4789–4797.